Russian Journal of Nonlinear Dynamics
Full-texts are available at http://nd.ics.org.ru
DOI: 10.20537/nd251201

NONLINEAR PHYSICS AND MECHANICS

MSC 2010: 70E40, 70E55, 70K44, 70K55

Perturbed Dynamics of the Lagrange Gyrostat

A. V. Doroshin, V. S. Aslanov

The attitude dynamics of the Lagrange gyrostat is considered. A dynamical analogy of the heavy Lagrange gyrostat and the magnetic Lagrange gyrostat satellite on a circle equatorial orbit in the geomagnetic field is shown. Analytical solutions for homoclinic and heteroclinic phase trajectories are obtained. Dynamical chaos is analyzed. The practical application of the Lagrange gyrostat in space flight dynamics is presented. The results of the paper can be especially applicable for small spacecraft and nanosatellites of space remote sensing constellations.

Keywords: Lagrange top, gyrostat, satellite, magnetic field, circle equatorial orbit, perturbed dynamics

1. Introduction

The problem of the dynamics of a heavy rigid body rotating about its fixed point in a planar gravity field represents an important part of theoretical mechanics. Significant results in this scientific area have been obtained by Alexey V. Borisov. His numerous works noticeably enriched and developed rigid body dynamics. First of all, mention should be made of the well-known monograph [1], co-authored by Ivan S. Mamaev, where the main classical and modern problems were collected and discussed. In addition, it is necessary to cite some works related to special topics of the regular and chaotic dynamics of rigid bodies [2–6].

One of the questions addressed by A. V. Borisov is the possibility of generalizing the classical cases of rigid body motion on the gyrostat system [1], and especially in the Lagrange case. In this connection, the authors fondly remember their personal discussions with A. V. Borisov about this problem, where the Lagrange gyrostat was considered not only in terms of integrability of its mathematical model, but also from the mechanical point of view and practical applications

Received August 28, 2025
Accepted November 25, 2025

This work was supported by the Russian Science Foundation (# 25-19-00312).

Anton V. Doroshin
doran@inbox.ru
Vladimir S. Aslanov
aslanov_vs@mail.ru
Samara National Research University
Moskovskoye sh. 34, Samara, 443086 Russia

in space flight tasks. Therefore, it is important to present in this paper some new results in the Lagrange gyrostat problem, and to underline the gratitude to Alexey Borisov for his opinion and suggestions.

As is well known, the Lagrange top is one of the classical cases of the angular motion of a heavy body around a fixed point. This case has been well observed in classical works, but it is not finalized in its own development. So, we should mention some papers with a multidirectional study of the Lagrange top [7–18], where many aspects of its dynamics are studied, including the symplectic structure, bifurcation analysis, resonance motions and cases with generalizations of the potential. The next research directions are concerned with the perturbed Lagrange top motion [19–26], where vibrating suspensions, small dynamical asymmetry and cases of principal nonintegrability are investigated. A transition to the topic of the Lagrange gyrostat and magnetic gyrostats was implemented in the works [27–36], where, among other things, the possible dynamical equivalence of the "heavy body" and the "magnetic body" is introduced [30], important analytical solutions and elliptic quadratures are obtained [27, 28, 34], and the practical applications of magnetic spacecraft and gyrostat satellites are proposed [35, 36].

2. The classical case of the heavy Lagrange gyrostat

At the beginning of our research, it is useful to present a short description of main results within the framework of the unperturbed Lagrange gyrostat [27], consisting of the main body and the rotor actuated by the internal torque (unbalanced gyrostat). The mechanical scheme of the system is presented in Fig. 1.

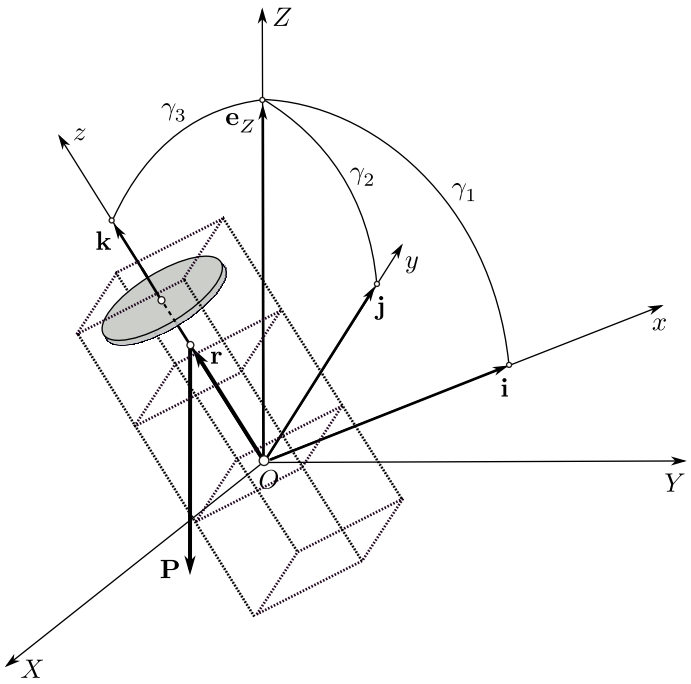

Fig. 1. The heavy Lagrange gyrostat: $OXYZ$ is an inertial coordinate system, $Oxyz$ is a coordinate system attached to the main body of the gyrostat

The equations of motion for the Lagrange gyrostat can be written on the basis of the angular momentum law:

$$\mathbf{J}\cdot\dot{\boldsymbol{\omega}}+\dot{\mathbf{h}}+\boldsymbol{\omega}\times(\mathbf{J}\cdot\boldsymbol{\omega}+\mathbf{h})=\mathbf{M} \tag{2.1}$$

where $\mathbf{J}=\mathrm{diag}[A,\,A,\,C]$ is the inertia tensor of the gyrostat as a whole system, including the main body and the immovable ("freezed") rotor; $\boldsymbol{\omega}=[p,\,q,\,r]^T$ is the absolute angular velocity of the main body of the gyrostat referred to the frame $Oxyz$, attached to the main body; $\mathbf{h}=[0,\,0,\,C_r\sigma]^T$ is the angular momentum of the rotor relative to the main body; σ is the longitudinal angular velocity of the rotor relative to the main body; C_r is the inertia moment of the rotor about the longitudinal axis Oz; $\mathbf{M}=[Pa\gamma_2,\,-Pa\gamma_1,\,0]^T$ is the external torque from the gyrostat weight $\mathbf{P}$; $\mathbf{r}=[0,\,0,\,a]^T$ is the vector of the point of application of weight $\mathbf{P}$; $\boldsymbol{\gamma}=[\gamma_1,\,\gamma_2,\,\gamma_3]^T$ are the directional cosines of the inertial "vertical" axis OZ.

The motion of the rotor is described by the following equation:

$$C_r(\dot r+\dot\sigma)=M_r \tag{2.2}$$

where M_r is the internal torque acting on the rotor from the side of the main body.

In the scalar form, Eq. (2.1) can be written as

$$\begin{cases} A\dot p+(C-A)qr+C_rq\sigma=Pa\gamma_2,\\ A\dot q+(A-C)pr-C_rp\sigma=-Pa\gamma_1,\\ C\dot r+C_r\dot\sigma=0,\quad C_r(\dot r+\dot\sigma)=M_r. \end{cases} \tag{2.3}$$

The kinematic equations represent the Poisson system:

$$\dot\gamma_1=r\gamma_2-q\gamma_3,\quad \dot\gamma_2=p\gamma_3-r\gamma_1,\quad \dot\gamma_3=q\gamma_1-p\gamma_2,\quad \dot\delta=\sigma \tag{2.4}$$

with one additional equation for the angle of relative rotation of the rotor, δ.

The following three classical first integrals will be actual for the system:

$$\gamma_1^2+\gamma_2^2+\gamma_3^2=1, \tag{2.5}$$

$$A(p\gamma_1+q\gamma_2)+(Cr+C_r\sigma)\gamma_3=K_Z, \tag{2.6}$$

$$Cr+C_r\sigma=K_z. \tag{2.7}$$

Integrals (2.6) and (2.7) define the conservation of the system's angular momentum referred to the axes OZ and Oz. The fourth integral follows from the kinetic energy theorem:

$$\frac12\left[A\left(p^2+q^2\right)+C_nr^2+C_r(r+\sigma)^2\right]-T_0=-Pa\gamma_3+\int_0^\delta M_r\,d\delta, \tag{2.8}$$

where C_n is the longitudinal inertia moments of the main body ($C_n=C-C_r$), $T_0=\frac12\left[A\left(p_0^2+\right.\right.$ $\left.\left.+q_0^2\right)+C_nr_0^2+C_r(r_0+\sigma_0)^2\right]$, and $p(0)=p_0$, $q(0)=q_0$, $r(0)=r_0$, $\sigma(0)=\sigma_0$ are the initial values of the angular velocity components.

To simplify the expression (2.8), we can rewrite [27] the last two of equations (2.3):

$$C_n\dot r=-M_r;\quad C_r(\dot r+\dot\sigma)=M_r. \tag{2.9}$$

Multiplication of Eqs. (2.9) by r and $(r+\sigma)$, respectively, and subsequent integration gives:

$$\frac{1}{2}C_n\,dr^2 = -M_r r\,dt, \quad \frac{1}{2}C_r\,d(r+\sigma)^2 = M_r(r+\sigma)\,dt.$$

The sum of the last expressions represents the work of the internal torque M_r:

$$\int\limits_0^\delta M_r\,d\delta = \frac{1}{2}\left[C_n r^2 + C_r(r+\sigma)^2\right] + \text{const} \quad (d\delta = \sigma\,dt) \tag{2.10}$$

and, therefore, the first integral (2.8) takes the form [27]:

$$\frac{A}{2}\left(p^2+q^2\right) + Pa\gamma_3 = \text{const} = h. \tag{2.11}$$

Here we should underline that the integral (2.11) will be fulfilled at any arbitrary internal torque M_r. These four integrals allow one to write analytical solutions for the Euler angles in elliptic functions and elliptic integrals under the action of an arbitrary internal torque M_r [27]:

$$\begin{cases} \cos\theta = (u_2-u_1)\,\mathrm{sn}^2(\beta t+\alpha,\,k) + u_1; \\ \psi = GI_1 - RI_2 + \psi_0; \\ \varphi = \int\limits_0^t r(t)\,dt - GI_2 + R(I_1 - t) + \varphi_0 \end{cases} \tag{2.12}$$

where the following constants take place:

$$\begin{cases} R = \dfrac{K_z}{A}; \quad G = \dfrac{K_Z}{A}; \quad H = \dfrac{h}{A}; \quad g = \dfrac{Pa}{A}; \\ \beta = \sqrt{\dfrac{g(u'-u_1)}{2}}; \quad k^2 = \dfrac{u_2-u_1}{u'-u_1}; \quad 0 \leqslant k^2 < 1; \\ I_1 = \dfrac{n_1\Pi(\xi,\,n_1,\,k) - n_2\Pi(\xi,\,n_2,\,k)}{2\beta(u_2-u_1)}; \quad I_2 = -\dfrac{n_1\Pi(\xi,\,n_1,\,k) + n_2\Pi(\xi,\,n_2,\,k)}{2\beta(u_2-u_1)}; \\ \xi = \mathrm{am}(z,\,k); \quad z = \beta t + \alpha; \quad n_1 = \dfrac{u_2-u_1}{1+u_1}; \quad n_2 = -\dfrac{u_2-u_1}{1-u_1}; \\ \Pi(\xi,\,n,\,k) = \overline{\Pi}(\xi,\,n,\,k) - \overline{\Pi}(\xi_0,\,n,\,k); \\ \overline{\Pi}(\xi,\,n,\,k) = \displaystyle\int\limits_0^\xi \frac{d\xi}{\left(1+n\sin^2\xi\right)\sqrt{1-k^2\sin^2\xi}}, \end{cases} \tag{2.13}$$

and u_1, u_2, u' are the roots $(-1 < u_1 \leqslant u_0 \leqslant u_2 < 1 < u' < \infty)$ of the polynomial $f(u) = (H - 2gu)\left(1-u^2\right) - (G-Ru)^2$.

The solutions (2.12) repeat, in general, the structure of the classical solutions for the Lagrange top as one single body, but in the case of the unbalanced Lagrange gyrostat we have not the constancy of the longitudinal angular velocity r, which now depends on time (2.9) due to the presence of the internal torque M_r:

$$r(t) = -\frac{1}{C_n}\int\limits_0^t M_r(t)\,dt + r_0. \tag{2.14}$$

Moreover, the form of the internal torque can be very complex, and can depend on all dynamical parameters:

$$M_r = M_r(t) = M_r(p(t),\, q(t),\, r(t),\, \sigma(t),\, \theta(t),\, \psi(t),\, \varphi(t),\, \delta(t)),$$

and, therefore, it cannot be said that the solutions (2.12) fully repeat the classical form for the Lagrange top. For this reason the solutions (2.12) are quite independent and are not identical to the classical ones (at least in terms of constants' values, of integral (2.8) form, and in the form of the intrinsic rotation angle $\varphi(t)$). So, this fact is important for practical applications, especially when it comes to the attitude dynamics of gyrostat satellites.

3. The Lagrange gyrostat as the satellite in a geomagnetic field

Let us consider the attitude motion of a satellite with a magnetic control system, which generates the own dipole magnetic moment $\mathbf{m}$ of the satellite. Then the satellite will interact with the external geomagnetic field during the motion of its center of mass along the orbit. If the orbital motion is implemented along the equatorial circular orbit, then we can consider the external geomagnetic induction as constant vector $\mathbf{B}_{\text{orb}}$, i.e., the geomagnetic field in this case is constant. This argument is followed from the approximate modeling of the geomagnetic field structure as the force surfaces of the Earth magnetic dipole $\mathbf{B}_{\oplus}$ (Fig. 2).

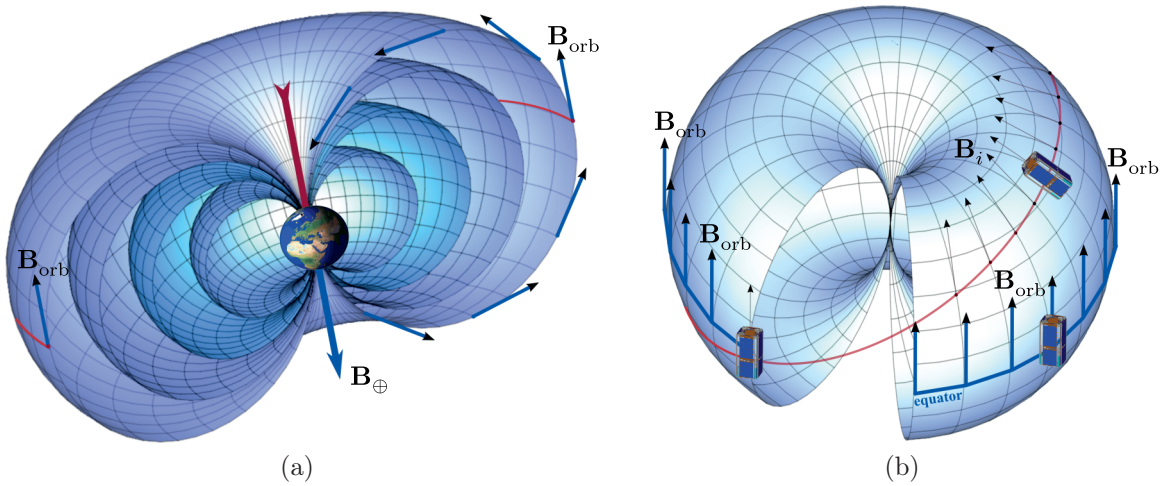

(a) (b)

Fig. 2. Force surfaces of the geomagnetic field (a) and the orbital motion of the satellite (b) along the equatorial circular orbit with a constant vector of geomagnetic induction

Obviously, for any inclined orbit the geomagnetic induction vector will be variable ($\mathbf{B}_i = = \mathbf{var}$). So, in the case of the circle equatorial orbit we get dynamical conditions similar to the Lagrange top case (Fig. 3), when the magnetic interaction plays the role of the gravitational torque:

$$\mathbf{M} = \mathbf{r} \times \mathbf{P} \quad \leftrightarrow \quad \mathbf{M} = \mathbf{m} \times \mathbf{B}_{\text{orb}}. \tag{3.1}$$

Therefore, under the condition ($mB_{\text{orb}} = -Pa$) the motion of the magnetic gyrostat will fully repeat the motion of the heavy gyrostat.

We will describe the attitude motion of the gyrostat satellite in Euler angles in the orbital frame $CXYZ$ with origin at the center of mass (Fig. 3). In this case, we will have the following

kinematic equations:

$$\begin{cases} p = \dot{\psi}\sin\theta\sin\varphi + \dot{\theta}\cos\varphi + \Omega\Theta_{13}; \\ q = \dot{\psi}\sin\theta\cos\varphi - \dot{\theta}\sin\varphi + \Omega\Theta_{23}; \\ r = \dot{\psi}\cos\theta + \dot{\varphi} + \Omega\Theta_{33}; \\ \sigma = \dot{\delta} \end{cases} \tag{3.2}$$

where Ω is the orbital angular velocity and Θ_{ij} are the components of the transition matrix between the orbital and the connected frames:

$$\Theta_{13} = \sin\varphi\sin\theta; \quad \Theta_{23} = \cos\varphi\sin\theta; \quad \Theta_{13} = \cos\theta. \tag{3.3}$$

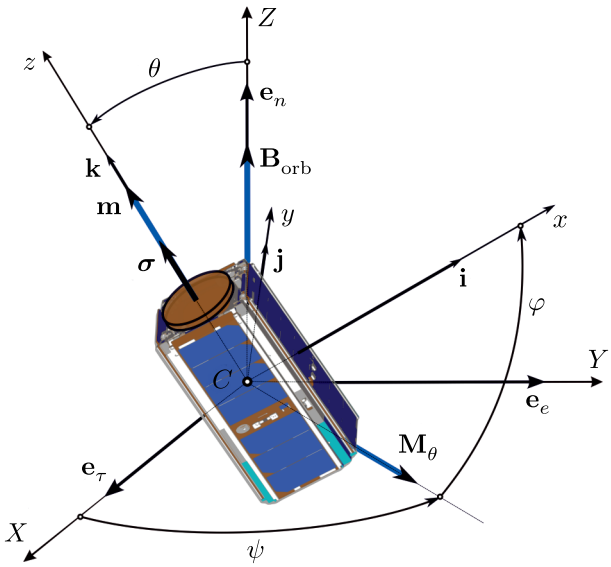

Fig. 3. The magnetic gyrostat satellite in the orbital frame $CXYZ$ under the dynamical conditions of the Lagrange top along the equatorial circular orbit

Let us derive canonical equations for the Euler angles. The canonical momenta are:

$$p_\theta = \frac{\partial T}{\partial\dot{\theta}}; \quad p_\psi = \frac{\partial T}{\partial\dot{\psi}}; \quad p_\varphi = \frac{\partial T}{\partial\dot{\varphi}}; \quad p_\delta = \frac{\partial T}{\partial\sigma}. \tag{3.4}$$

Then, differentiating the kinetic energy and using (3.2), we can write the so-called conjunctional expressions:

$$\begin{cases} \widehat{\dot{\theta}} = \dfrac{p_\theta}{A}; \quad \widehat{\dot{\varphi}} = \dfrac{\left(A\sin^2\theta + C_n\cos^2\theta\right)p_\varphi - Ap_\delta\sin^2\theta - C_n p_\psi\cos\theta}{AC_n\sin^2\theta}; \\ \widehat{\dot{\psi}} = \dfrac{p_\psi - A\Omega\sin^2\theta - p_\varphi\cos\theta}{A\sin^2\theta}; \quad \widehat{\dot{\delta}} = \widehat{\sigma} = \dfrac{C_r(p_\delta - p_\varphi) + C_n p_\delta}{C_r C_n}. \end{cases} \tag{3.5}$$

Then the kinetic energy can be rewritten as

$$\widehat{T} = \frac{(p_\varphi\cos\theta - p_\psi)^2}{2A\sin^2\theta} + \frac{C_n p_\theta^2 + A(p_\varphi - p_\delta)^2}{2AC_n} + \frac{p_\delta^2}{2C_r}. \tag{3.6}$$

The potential energy has the form

$$P = -\int |\mathbf{m}| \cdot |\mathbf{B}_{\rm orb}| \sin\vartheta \, d\vartheta = |\mathbf{m}| \cdot |\mathbf{B}_{\rm orb}| \cos\vartheta = \mathbf{m} \cdot \mathbf{B}_{\rm orb} = mB_{\rm orb} \cos\theta. \tag{3.7}$$

Then the Hamiltonian of the magnetic Lagrange gyrostat satellite is

$$\mathcal{H} = \sum_i p_i \, \widehat{\dot{q}}_i - L(q_i, \, \widehat{\dot{q}}_i) = \\ = \frac{(p_\varphi \cos\theta - p_\psi)^2}{2A \sin^2\theta} + \frac{C_n p_\theta^2 + A(p_\varphi - p_\delta)^2}{2AC_n} + \frac{p_\delta^2}{2C_r} - \Omega p_\psi + mB_{\rm orb} \cos\theta. \tag{3.8}$$

The Hamiltonian (3.8) generates the corresponding canonical equations (here we do not write their explicit forms):

$$\dot{q}_i = \frac{\partial \mathcal{H}}{\partial p_i}; \quad \dot{p}_i = -\frac{\partial \mathcal{H}}{\partial q_i}; \quad q_i = \{\theta, \, \psi, \, \varphi, \, \delta\}. \tag{3.9}$$

Equations (3.9) will describe the unperturbed dynamics of the Lagrange gyrostat in the conservative case without the internal torque M_r acting between the main body and the rotor, and, therefore, with constant longitudinal angular velocities of the main body and the rotor ($r = r_0$; $\sigma = \sigma_0$).

If we add the internal torque M_r then the equations for the intrinsic rotation angle and for the momentum of the relative rotor rotation take the form

$$\begin{cases} \dot{p}_\delta = M_r(t); \\ \dot{\varphi} = \dfrac{p_\varphi \cos^2\theta - p_\psi \cos\theta}{A \sin^2\theta} + \dfrac{p_\varphi - p_\delta(t)}{C_n}. \end{cases} \tag{3.10}$$

It follows from (3.10) that it is possible to control the trend of the intrinsic rotation. As the simplest example, if we produce the internal torque in the form

$$M_r(t) = M_{\rm spin} \cdot (H(t) - H(t - T_{\rm spin})) + G\omega_\delta \cos(\omega_\delta t) \tag{3.11}$$

then we can compensate for the growth of the average value of the angle φ and its oscillating parameters. In the law (3.11), the rotor spin-up part of the torque and the rotor oscillating part of the torque are presented, where $M_{\rm spin}$ is the value of the spin-up torque, $H(\cdot)$ is the Heaviside function, $T_{\rm spin}$ is the duration of the rotor spin-up process, G and ω_δ are the amplitude and frequency of generated oscillations of the rotor. With the torque (3.11) the time dependence for the momentum of the relative rotor rotation after the spin-up process (after time $T_{\rm spin}$) will correspond to the expression

$$p_\delta(t) = p_{\delta 0} + M_{\rm spin} T_{\rm spin} + G \sin\omega_\delta t. \tag{3.12}$$

The momentum p_δ produced by the internal torque (3.12) will change the trend of the intrinsic rotation angle due to the second of Eqs. (3.10). This dynamical possibility can be used to control the intrinsic rotation by the simplest tools. When it comes to the gyrostat satellite, the control of the rotor rotation by the internal spin-up electromotor can control the intrinsic rotation of the main body. This dynamical aspect can be applied within the framework of the remote sensing

of the Earth (Fig. 4). In this case the scanning camera is placed on the longitudinal axis on the opposite (to the rotor) side of the satellite. The nutational-precessional motion will direct the scanning camera, and the internal electromotor of the rotor will control the axial rotation of the camera and images received by it. Under real conditions this possibility can be more accessible in the cases with using feedback control, when the internal torque is formed by the control system in an appropriate form. Moreover, the parameters of the nutational and the precessional motion also can be changed by the feedback control by creating the corresponding value of the dipole moment m, defining the value of the restoring torque $\mathbf{M}_\theta$.

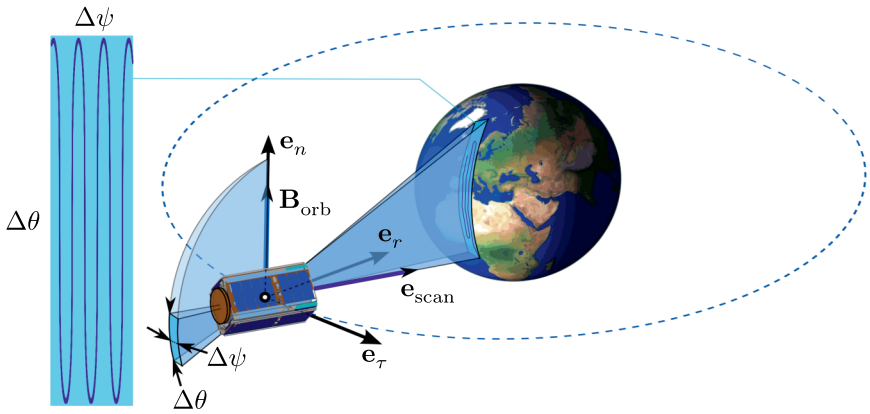

Fig. 4. The remote sensing of the Earth during the controlled angular motion of the magnetic Lagrange gyrostat satellite: the angular motion forming the scan route and the final image strip

The results of simple modeling are depicted in Figs. 5, 6, where the scan route and intrinsic rotation (the camera's axial rotation) was formed by the simplest internal torque (3.11). It should be noted that in this paper we use hypothetical values of all parameters, which do not correspond to natural values (B_{orb}, m, inertia moments, initial conditions), but it was allowed to show the qualitative side of the phenomena; and a concrete quantitative analysis with real processes is a separate engineering problem.

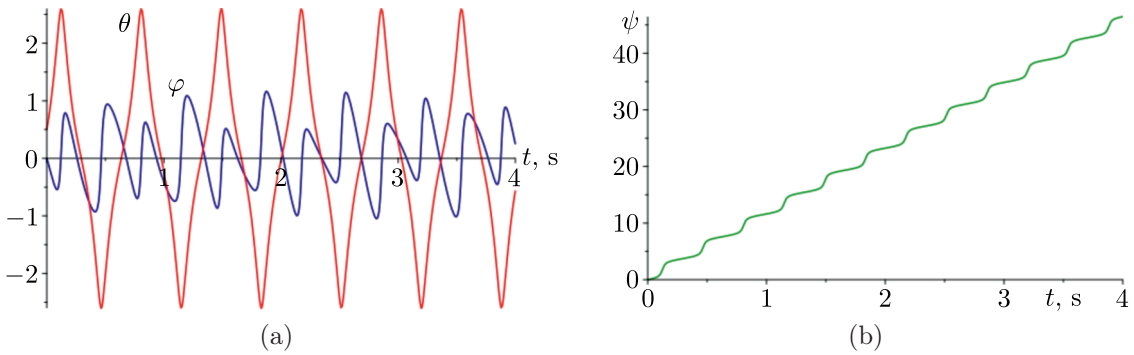

Fig. 5. Time-dependencies for the nutation θ (red), the intrinsic rotation φ (blue), the precession (green) angles during a hypothetical remote sensing process with the torque (3.11)

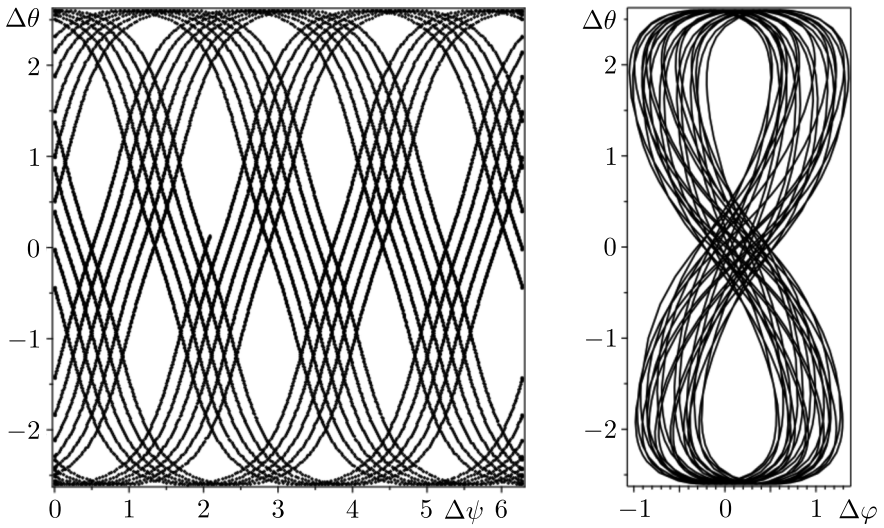

Fig. 6. The coverage of the scanning strip during the angular motion: (a) the strip $\{\Delta\psi,\, \Delta\theta\}$ and (b) the intrinsic rotation hodograph $\{\Delta\varphi,\, \Delta\theta\}$

Table 1. Numerical parameters for calculations (Figs. 5, 6)

A $[\mathrm{kg}\cdot\mathrm{m}^2]$	C_n $[\mathrm{kg}\cdot\mathrm{m}^2]$	C_r $[\mathrm{kg}\cdot\mathrm{m}^2]$	$m_1 B_{\mathrm{orb}}$ $[\mathrm{N}\cdot\mathrm{m}]$	p_ψ $[\mathrm{kg}\cdot\mathrm{m}^2/s]$	p_φ $[\mathrm{kg}\cdot\mathrm{m}^2/s]$	p_δ $[\mathrm{kg}\cdot\mathrm{m}^2/s]$	Ω $[1/s]$	ω_δ $[1/s]$	G $[\mathrm{kg}\cdot\mathrm{m}^2/s]$	$M_{\mathrm{spin}}T_{\mathrm{spin}}$ $[\mathrm{kg}\cdot\mathrm{m}^2/s]$
0.5	0.6	0.2	100	4	4	4	0.001	10	2	2.05

4. The perturbed dynamics of the magnetic Lagrange gyrostat satellite

In this section, we proceed to a development of the Lagrange gyrostat satellite case by some complication in the dependence for magnetic dipole m, which is formed by the control system and magnetic actuators (e. g., magnetic coils), and in the general case can have any form:

$$m = \mathrm{var} = m(q_i,\, p_i,\, t). \tag{4.1}$$

This complication significantly generalizes the classical problem of the Lagrange gyrostat, and defines a new broad research problem.

In this paper, we consider only one case of generalization, which corresponds to the so-called biharmonic restoring torque $\mathbf{M}_\theta$ [18]. Let us consider the dependence for the dipole moment, which is formed by the control system, in the following form:

$$m = m(\theta) = m_1 + m_2 \cos\theta \tag{4.2}$$

where m_1, m_2 are some constants. Then we obtain the biharmonic potential energy:

$$P = mB_{\mathrm{orb}} \cos\theta = m_1 B_{\mathrm{orb}} \cos\theta + m_2 B_{\mathrm{orb}} \cos^2\theta. \tag{4.3}$$

The corresponding Hamiltonian can be written as

$$\mathcal{H} = \frac{(p_\varphi \cos\theta - p_\psi)^2}{2A\sin^2\theta} + \frac{C_n p_\theta^2 + A(p_\varphi - p_\delta)^2}{2AC_n} + \frac{p_\delta^2}{2C_r} - \Omega p_\psi + m_1 B_{\mathrm{orb}} \cos\theta + m_2 B_{\mathrm{orb}} \cos^2\theta. \tag{4.4}$$

A complete study of the dynamics in this case is a complex analytical investigation which can involve obtaining analytical solutions, considering the phase portrait of the system and its bifurcations, introducing action-angle variables, etc.

In this paper, we focus only on searching for homo- and heteroclinic phase trajectories, which are very important in research into the chaotic dynamics.

Moreover, in the following analysis we assume that the equality of constant canonical momenta takes place:

$$p_\varphi = p_\psi. \tag{4.5}$$

Condition (4.5) enables the emergence of saddle points in the phase portrait in the plane $\{\theta, p_\theta\}$. The concrete form of the phase portrait and locations of saddle points in it can be studied by investigating the generalized potential:

$$\Pi(\theta) = \mathcal{H}\big|_{p_\theta \to 0} = \frac{p_\varphi^2(\cos\theta - 1)^2}{2A\sin^2\theta} + \frac{A(p_\varphi - p_\delta)^2}{2AC_n} + \frac{p_\delta^2}{2C_r} - \Omega p_\varphi + m_1 B_{\text{orb}}\cos\theta + m_2 B_{\text{orb}}\cos^2\theta. \tag{4.6}$$

The generalized potential depends on the set of values of constants and their relationships, which can be studied in detail. We will not analyze this complete bifurcation structure; instead, we consider three concrete possible cases.

4.1. Case 1

Let us assume that the form of the potential (4.6) corresponds to Fig. 7. In this case, the phase portrait has two symmetric (left and right) homoclinic trajectories with a common saddle point at $\theta = 0$, $p_\theta = 0$.

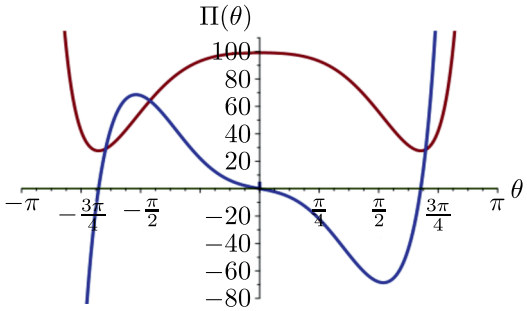

Fig. 7. The first form of the generalized potential (red) and its derivative (blue)

Table 2. Parameters for calculations of case 1

A $[\text{kg}\cdot\text{m}^2]$	C_n $[\text{kg}\cdot\text{m}^2]$	C_r $[\text{kg}\cdot\text{m}^2]$	$m_1 B_{\text{orb}}$ $[\text{N}\cdot\text{m}]$	$m_2 B_{\text{orb}}$ $[\text{N}\cdot\text{m}]$	p_ψ $[\text{kg}\cdot\text{m}^2/\text{s}]$	p_φ $[\text{kg}\cdot\text{m}^2/\text{s}]$	p_δ $[\text{kg}\cdot\text{m}^2/\text{s}]$	Ω [1/s]
0.5	0.6	0.2	100	−45.85	4	4	4	0.001

The value of the Hamiltonian (4.4) at the saddle point under condition (4.5) is

$$h^* = \frac{(p_\varphi - p_\delta)^2}{2C_n} + \frac{p_\delta^2}{2C_r} - \Omega p_\varphi + m_1 B_{\text{orb}} + m_2 B_{\text{orb}}. \tag{4.7}$$

The phase trajectory with energy value (4.7) will be described by the equation ($\mathcal{H} - h^* = 0$):

$$\frac{\left(p_\theta^2 - 2m_2 B_{\text{orb}} A \sin^2\theta - p_\varphi^2\right)\cos\theta - 2A(m_1 B_{\text{orb}} + m_2 B_{\text{orb}})\sin^2\theta + p_\varphi^2 + p_\theta^2}{2A(\cos\theta + 1)} = 0. \tag{4.8}$$

From Eq. (4.8) we obtain the dependence for the canonical momentum:

$$p_\theta = \pm\frac{1}{\sin\theta}\sqrt{2m_2 B_{\text{orb}} A \sin^4\theta - 2m_1 B_{\text{orb}} A(\cos\theta - 1)\sin^2\theta - p_\varphi^2(\cos\theta - 1)^2}. \tag{4.9}$$

The canonical differential equation for momentum p_θ at the condition (4.5) has the form

$$\dot{p}_\theta = \left(2Am_2 B_{\text{orb}}\cos^3\theta + A(m_1 B_{\text{orb}} + 4m_2 B_{\text{orb}})\cos^2\theta + \right.$$
$$\left. + 2A(m_1 B_{\text{orb}} + m_2 B_{\text{orb}})\cos\theta + m_1 B_{\text{orb}} A - p_\varphi^2\right)\frac{\sin\theta}{A(\cos\theta + 1)^2}. \tag{4.10}$$

Now we change the variable:

$$u = \cos\theta. \tag{4.11}$$

Then Eq. (4.10) takes the form

$$\dot{p}_\theta = \frac{\sqrt{1-u^2}}{A(u+1)^2}\left(2Am_2 B_{\text{orb}} u^3 + A(m_1 B_{\text{orb}} + 4m_2 B_{\text{orb}})u^2 + \right.$$
$$\left. + 2A(m_2 B_{\text{orb}} + m_1 B_{\text{orb}})u + m_1 B_{\text{orb}} A - p_\varphi^2\right). \tag{4.12}$$

The expression (4.9) with the new variable can be rewritten as

$$p_\theta(u) = \pm\frac{\sqrt{2\left((u+1)(m_2 B_{\text{orb}} u + m_1 B_{\text{orb}} + m_2 B_{\text{orb}})A - \frac{p_\varphi^2}{2}\right)(u-1)^2}}{\sqrt{1-u^2}}. \tag{4.13}$$

Differentiating (4.13) with respect to time gives

$$\dot{p}_\theta = \frac{\partial p_\theta}{\partial u}\dot{u} = \pm\frac{\sqrt{2}(u-1)\left((u+1)^2\left(m_2 B_{\text{orb}} u + \frac{m_1 B_{\text{orb}}}{2}\right)A - \frac{p_\varphi^2}{2}\right)}{(u+1)\sqrt{1-u^2}\sqrt{\left(A(u+1)(m_2 B_{\text{orb}} u + m_1 B_{\text{orb}} + m_2 B_{\text{orb}}) - \frac{p_\varphi^2}{2}\right)(u-1)^2}}\dot{u}. \tag{4.14}$$

Equating (4.14) and (4.12) and separating the differentials, we obtain

$$\frac{du}{(u-1)\cdot\sqrt{\left((u+1)\left(m_2 B_{\text{orb}} u + m_1 B_{\text{orb}} + m_2 B_{\text{orb}}\right)A - \frac{p_\varphi^2}{2}\right)}} = \mp\frac{\sqrt{2}\,dt}{A}. \tag{4.15}$$

Integrating Eq. (4.15) gives

$$F(u) - F(u_0) = \mp\frac{\sqrt{2}t}{A}, \tag{4.16}$$

where

$$F(u) = \frac{2}{\sqrt{s_1}}\ln\left(\frac{2s_1 + s_2(u-1) + 2\sqrt{s_1}\sqrt{4A(u-1)^2 m_2 B_{\text{orb}} + s_2 u + s_1 - s_2}}{u-1}\right); \tag{4.17}$$

$$s_1 = 8AB_{\text{orb}}(m_1 + m_2) + 8m_2 B_{\text{orb}} A - 2p_\varphi^2; \quad s_2 = 4AB_{\text{orb}}(m_1 + m_2) + 12m_2 B_{\text{orb}} A.$$

The value u_0 is the initial condition of the motion along the homoclinic trajectory; it corresponds to the point where the trajectory crosses the axis for the θ-variable in the phase portrait, i. e. when $p_\theta = 0$ at $\theta \neq 0$ (due to the symmetry properties). Therefore, this value will correspond to the solution of the equation following from (4.13):

$$(u_0+1)(m_2 B_{\text{orb}} u_0 + m_1 B_{\text{orb}} + m_2 B_{\text{orb}})A - \frac{p_\varphi^2}{2} = 0. \tag{4.18}$$

The appropriate solution to (4.18) is

$$u_0 = -\frac{m_1 B_{\text{orb}} A + 2m_2 B_{\text{orb}} A \mp \sqrt{A^2 m_1^2 B_{\text{orb}}^2 + 2A p_\varphi^2 m_2 B_{\text{orb}}}}{2m_2 B_{\text{orb}} A}. \tag{4.19}$$

The final analytical solution for $u(t)$ follows from (4.16) after inversion of functions:

$$u(t) = \frac{16m_2 B_{\text{orb}} A s_1 - s_2^2 + (2s_2 - 4s_1) e^{\frac{-\sqrt{s_1}\left(AF(u_0) \mp \sqrt{2}t\right)}{2A}} - e^{\frac{-\sqrt{s_1}\left(AF(u_0) \mp \sqrt{2}t\right)}{A}}}{16m_2 B_{\text{orb}} A s_1 - s_2^2 + 2s_2 e^{\frac{-\sqrt{s_1}\left(AF(u_0) \mp \sqrt{2}t\right)}{2A}} - e^{\frac{-\sqrt{s_1}\left(AF(u_0) \mp \sqrt{2}t\right)}{A}}}. \tag{4.20}$$

Then we have the analytical solutions (4.20) for $\cos\theta$ and for canonical momentum (4.13), which are linked with the homoclinic trajectory.

Now we numerically confirm the analytical solutions and plot the corresponding phase portrait $\{\theta,\, p_\theta\}$ (Figs. 8, 9), where the axis for momentum p_θ is scaled for the maximum value $p_\theta = 30\ \left[\text{kg}\cdot\text{m}^2/s\right]$.

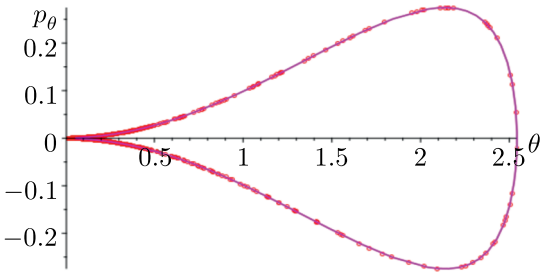

Fig. 8. The homoclinic trajectory of case 1: the magenta line is the analytical solution, and the red dots indicate numerical calculations

Here we need to note that similar homoclinic solutions under the dynamical conditions of this case were presented in [26]. The solutions [26] correspond to the classical Lagrange top:

$$\begin{cases} u(t) = \cos\theta = 1 - \gamma\,\text{sech}\left(\dfrac{\sqrt{\beta\gamma}}{2}t\right)^2; \\ \gamma = 2 - \dfrac{\left(\frac{p_\varphi}{A}\right)^2}{\frac{2mgl}{A}}; \quad \beta = \dfrac{2mgl}{A}; \quad b = \dfrac{p_\varphi}{A}; \quad mgl = m_1 B_{\text{orb}}. \end{cases} \tag{4.21}$$

The new analytical solutions (4.20) generalize solutions (4.21); as the value $m_2 B_{\text{orb}}$ decreases, the new solutions get closer to (4.21) — this can be observed in Fig. 10.

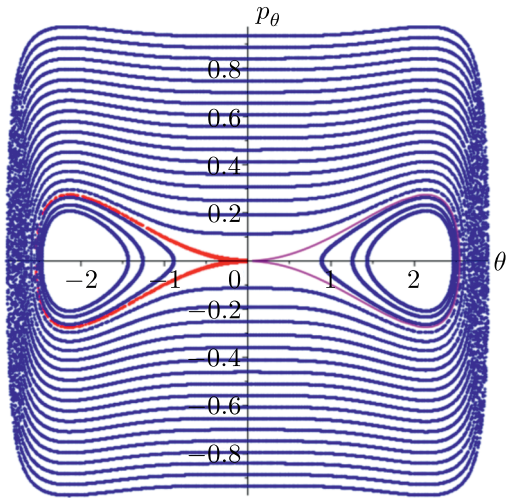

Fig. 9. The phase portrait of case 1: the left homoclinic trajectory (the red line) is numerical, and the right trajectory (the magenta line) is analytical

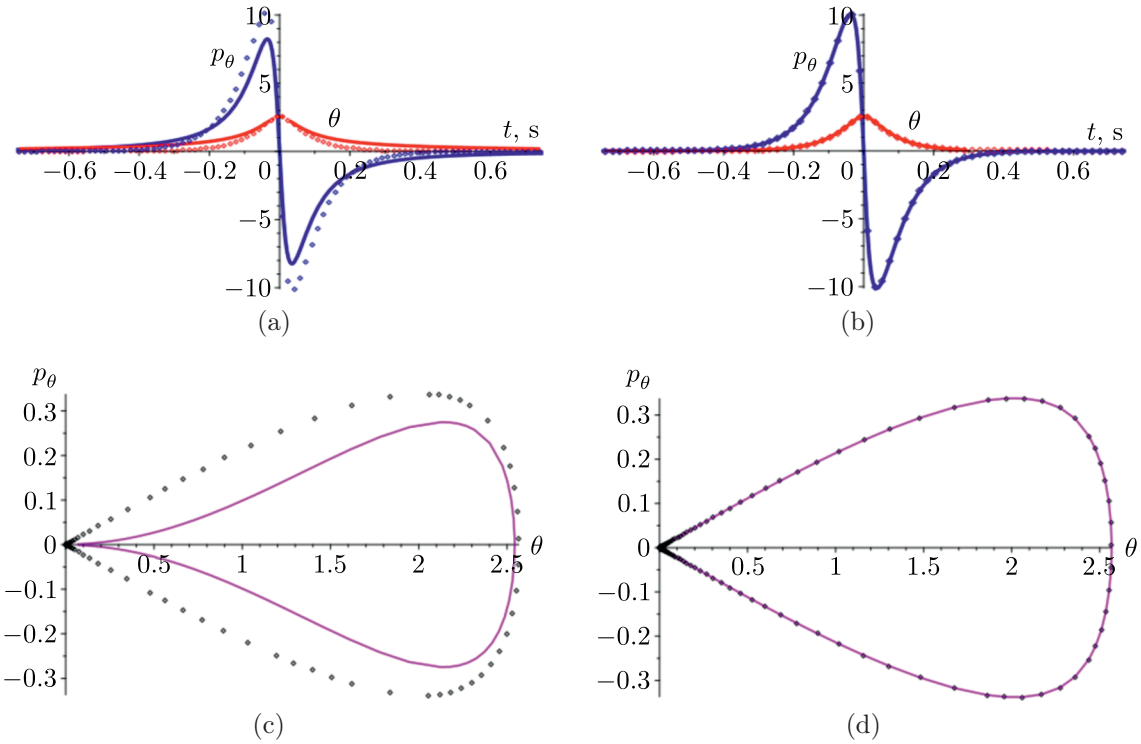

Fig. 10. Comparison of solutions (4.20) (lines) and (4.21) (dots): (a) the dependences for θ (red) and for p_θ (blue) at $m_2 B_{\text{orb}} = -45.85$ [N · m]; (b) the dependences for θ (red) and for p_θ (blue) at $m_2 B_{\text{orb}} = -0.4585$ [N · m]; (c) the homoclinic trajectory of the phase portrait $\{\theta, p_\theta\}$ at $m_2 B_{\text{orb}} = -45.85$ [N · m]; (d) the homoclinic trajectory of the phase portrait $\{\theta, p_\theta\}$ at $m_2 B_{\text{orb}} = -0.4585$ [N · m]

4.2. Case 2

Assume that the form of the potential (4.6) corresponds to Fig. 11. In this case, the phase portrait has two symmetrical (upper and lower) heteroclinic trajectories with different saddle

points. Moreover, as we can see from Fig. 11, the roots of the potential derivative are multiples (we need this to analytically integrate the solution).

This case is satisfied under the following constraints:

$$Am_1B_{\text{orb}} = p_\varphi^2. \tag{4.22}$$

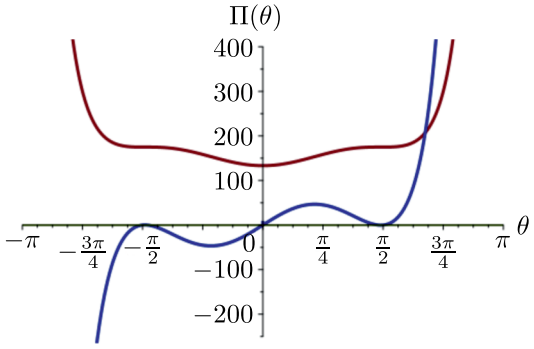

Fig. 11. The second form of the generalized potential (red) and its derivative (blue)

Table 3. Parameters for calculations for case 2

A $[\text{kg}\cdot\text{m}^2]$	C_n $[\text{kg}\cdot\text{m}^2]$	C_r $[\text{kg}\cdot\text{m}^2]$	m_1B_{orb} [N · m]	m_2B_{orb} [N · m]	p_ψ $[\text{kg}\cdot\text{m}^2/\text{s}]$	p_φ $[\text{kg}\cdot\text{m}^2/\text{s}]$	p_δ $[\text{kg}\cdot\text{m}^2/\text{s}]$	Ω [1/s]
0.5	0.6	0.2	100	−45.85	7.071	7.071	7.071	0.001

As we can see from Fig. 11, the center point will be located at $\theta = p_\theta = 0$ and two saddle points will symmetrically surround the center. The location of saddle points can be found from the solution of the generalized potential derivative:

$$\frac{\partial\Pi}{\partial\theta} = -\frac{\sin\theta\left(2m_2B_{\text{orb}}\cos^2\theta + (m_1B_{\text{orb}} + 4m_2B_{\text{orb}})\cos\theta + 2m_1B_{\text{orb}} + 2m_2B_{\text{orb}}\right)\cos\theta}{(\cos\theta+1)^2} = 0. \tag{4.23}$$

The appropriate roots of (4.23) are

$$\cos\theta^* = u^* = \frac{-m_1 - 4m_2 \mp \sqrt{m_1^2 - 8m_1m_2}}{4m_2}. \tag{4.24}$$

Then we can calculate the value of the energy along the heteroclinic trajectory connecting these two saddle points $h^* = \mathcal{H}\big|_{\{p_\theta\to 0;\ \theta\to\theta^*\}}$. The dependence of the canonical momentum on the coordinate (after the change of variable $\cos\theta = u$) takes the form

$$\begin{aligned} p_\theta(u) = \frac{\sqrt{A}}{\sqrt{C_rC_n(u+1)}}\Big[&2C_r(C_n\Omega + p_\delta)(u+1)\sqrt{Am_1B_{\text{orb}}} - p_\delta^2(u+1)C_n - \\ &- \left(2u^3m_2B_{\text{orb}} + 2B_{\text{orb}}(m_1+m_2)u^2 + (m_1B_{\text{orb}} - 2h^*)\,u - 2h^* + m_1B_{\text{orb}}\right)C_rC_n - \\ &-(u+1)\left(Am_1B_{\text{orb}} + p_\delta^2\right)C_r\Big]. \end{aligned} \tag{4.25}$$

The canonical differential equation for momentum p_θ in the case considered is

$$\dot{p}_\theta = \frac{u\sqrt{1-u^2}\left(2m_2B_{\text{orb}}u^2 + (m_1B_{\text{orb}} + 4m_2B_{\text{orb}})u + 2B_{\text{orb}}(m_1+m_2)\right)}{(u+1)^2}. \tag{4.26}$$

After differentiating (4.25) with respect to time and after equating with (4.26), we obtain the differential equation for u:

$$-\frac{AC_nC_r\,du}{\sqrt{\text{poly}_3(u)}} = \sqrt{1-u}\,dt \tag{4.27}$$

where

$$\begin{aligned}\text{poly}_3(u) = -AC_nC_r\Big[&-2C_1(C_n\Omega + p_\delta)(u+1)\sqrt{Am_1B_{\text{orb}}} + p_\delta^2(u+1)C_n + \\ &+ \left(\left(2u^3m_2B_{\text{orb}} + 2B_{\text{orb}}(m_1+m_2)u^2 + (m_1B_{\text{orb}} - 2h^*)\,u - 2h^* + m_1B_{\text{orb}}\right)C_n + \right. \\ &\left. + (u+1)\left(Am_1B_{\text{orb}} + p_\delta^2\right)\right)C_r\Big].\end{aligned}$$

The polynomial $\text{poly}_3(u)$ has one simple (U_1) and two multiple (U_2) roots (Fig. 12).

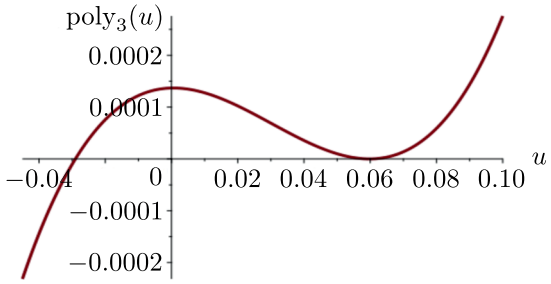

Fig. 12. The polynomial $\text{poly}_3(u)$ and its roots

After the expansion of the polynomial $\text{poly}_3(u)$ into roots, Eq. (4.27) can be rewritten as

$$-\frac{2AC_n\,du}{(u-U_2)\sqrt{-2AC_n^2C_r^2m_2B_{\text{orb}}(u-U_1)(1-u)}} = 2\,dt. \tag{4.28}$$

After integrating, we can write the solution:

$$F(u) - F(u_0) = 2t, \tag{4.29}$$

where

$$\begin{aligned}F(u) = &\frac{AC_n\sqrt{2}}{\sqrt{AC_n^2C_r^2m_2B_{\text{orb}}(U_2-1)(U_2-U_1)}}\times \\ &\times\ln\left[\frac{4AC_n^2C_r^2m_2B_{\text{orb}}\sqrt{(U_2-1)(U_2-U_1)}\sqrt{(u-U_1)(u-1)}}{u-U_2} - \right. \\ &\left. - \frac{2A((u+U_2-2)U_1 + (1-2U_2)u + U_2)C_r^2C_n^2m_2B_{\text{orb}}}{u-U_2}\right].\end{aligned} \tag{4.30}$$

The initial condition for u_0 corresponds to $\theta_0 = 0$ due to symmetry of the heteroclinic trajectory, and, therefore, $u_0 = 1$.

In this case, the final analytical solution after inversions of functions is

$$u(t) = \frac{f_1(t) + f_2(t)}{f_3(t) + f_4(t)}, \tag{4.31}$$

where

$$f_1(t) = -4Am_2B_{\text{orb}}C_r^2C_n^2((U_2-2)U_1+U_2)e^{\frac{v(t)}{AC_n\sqrt{2}}};$$
$$f_2(t) = 4U_2\left(\frac{1}{4}e^{\frac{\sqrt{2}v(t)}{AC_n}} + A^2C_r^4C_n^4m_2^2B_{\text{orb}}^2(U_1-1)^2\right);$$
$$f_3(t) = 4Am_2B_{\text{orb}}C_r^2C_n^2(U_1-2U_2+1)e^{\frac{v(t)}{AC_n\sqrt{2}}};$$
$$f_4(t) = e^{\frac{\sqrt{2}v(t)}{AC_n}} + 4A^2C_r^4C_n^4m_2^2B_{\text{orb}}^2(U_1-1)^2;$$
$$v(t) = \sqrt{Am_2B_{\text{orb}}C_r^2C_n^2(U_2-1)(U_2-U_1)}(2t+F(1)).$$

So, now we have the final analytical solution (4.31) for $\cos\theta$ and for momentum (4.25). The numerical confirmation of the analytical solutions and the phase portrait $\{\theta,\, p_\theta\}$ are presented in Figs. 13, 14, where the axis for momentum p_θ is scaled for the maximum value $p_\theta = 30\ \left[\text{kg}\cdot\text{m}^2/\text{s}\right]$.

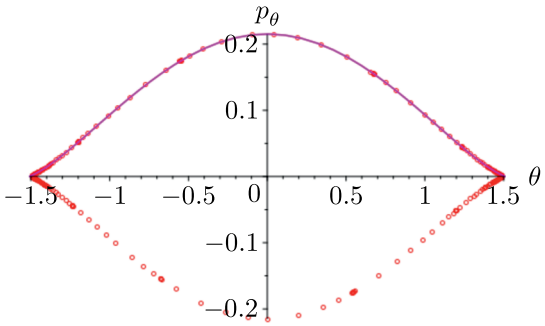

Fig. 13. The homoclinic trajectory of case 2: the magenta line is the analytical solution, and the red dots indicate numerical calculations

4.3. Case 3

Assume that the form of the potential (4.6) corresponds to Fig. 15. In this case, the phase portrait has two symmetrical (upper and lower) heteroclinic/homoclinic trajectories with saddle points $\left\{\theta_1^* = 0;\, p_\theta = 0\right\}$ and $\left\{\theta_1^* = 2\pi;\, p_\theta = 0\right\}$. The 2π-periodic repetition of the saddle points allows one to consider the trajectory connecting saddles as homoclinic and as heteroclinic.

This case is fulfilled under the following constraints:

$$p_\psi = p_\varphi = 0. \tag{4.32}$$

In this case, the value of energy along the homoclinic trajectory is

$$h^* = \frac{p_\delta^2(C_r + C_n)}{2C_nC_r} + m_1B_{\text{orb}} + m_2B_{\text{orb}}. \tag{4.33}$$

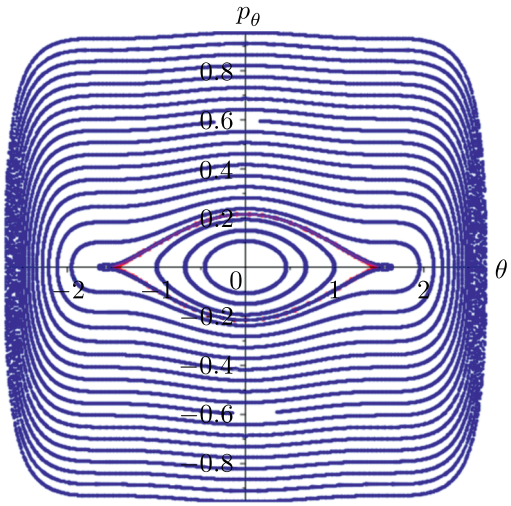

Fig. 14. The phase portrait of case 2: the upper heteroclinic trajectory (the magenta line) is analytical, and the lower trajectory (the red line) is numerical

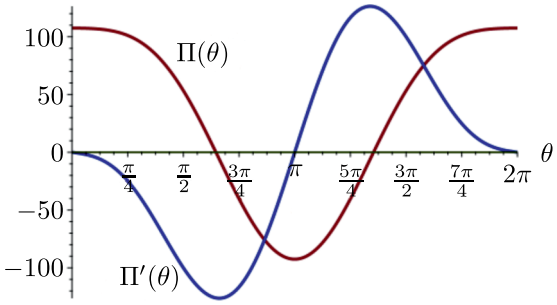

Fig. 15. The third form of the generalized potential (red) and its derivative (blue)

Table 4. Parameters for calculation for case 3

A $[\text{kg}\cdot\text{m}^2]$	C_n $[\text{kg}\cdot\text{m}^2]$	C_r $[\text{kg}\cdot\text{m}^2]$	m_1B_{orb} $[\text{N}\cdot\text{m}]$	m_2B_{orb} $[\text{N}\cdot\text{m}]$	p_ψ $[\text{kg}\cdot\text{m}^2/\text{s}]$	p_φ $[\text{kg}\cdot\text{m}^2/\text{s}]$	p_δ $[\text{kg}\cdot\text{m}^2/\text{s}]$	Ω [1/s]
0.5	0.6	0.2	100	−45.85	0	0	4	0.001

The dependence for the momentum on the coordinate ($\cos\theta = u$) has the form

$$p_\theta(u) = \frac{\sqrt{2Am_2B_{\text{orb}}\left(1-u^2\right)^2 - 2Am_1B_{\text{orb}}u\left(1-u^2\right) + 2Am_1B_{\text{orb}}\left(1-u^2\right)}}{\sqrt{1-u^2}}. \tag{4.34}$$

The canonical equation is

$$\dot{p}_\theta = \sqrt{1-u^2}(2m_2B_{\text{orb}}u + m_1B_{\text{orb}}). \tag{4.35}$$

Differentiating Eq. (4.34) with respect to time, we obtain

$$\dot{p}_\theta = \frac{A\sqrt{2}(u-1)\left(m_2B_{\text{orb}}u + \frac{1}{2}m_1B_{\text{orb}}\right)(u+1)\dot{u}}{\sqrt{A(u+1)(u-1)^2(m_2B_{\text{orb}}u + m_1B_{\text{orb}} + m_2B_{\text{orb}})}\sqrt{1-u^2}}. \tag{4.36}$$

After equating (4.36) with (4.35), we obtain the differential equation for u:

$$\frac{du}{(u-1)\sqrt{-m_2 B_{\text{orb}}(u+1)(b-u)}} = -\sqrt{\frac{2}{A}}\,dt, \tag{4.37}$$

where $b = -\frac{m_1+m_2}{m_2}$. Integrating Eq. (4.37) gives

$$F(u) - F(u_0) = -\sqrt{\frac{2}{A}}t \tag{4.38}$$

where

$$F(u) = -\frac{1}{\sqrt{2m_2 B_{\text{orb}}(1-b)}}\times \\ \times \ln\left(\frac{2\sqrt{2m_2 B_{\text{orb}}(1-b)}\sqrt{(u+1)m_2 B_{\text{orb}}(u-b)} - ((b-3)u+3b-1)m_2 B_{\text{orb}}}{u-1}\right).$$

The initial condition for u_0 corresponds to $\theta_0 = \pi$, and, therefore, $u_0 = -1$. The final solution follows after inversion of functions:

$$u(t) = \frac{(2-6b)e^{\frac{2t\sqrt{m_2 B_{\text{orb}}(1-b)}}{\sqrt{A}}} + \left(e^{\frac{4t\sqrt{m_2 B_{\text{orb}}(1-b)}}{\sqrt{A}}} + 1\right)(b+1)}{(2b-6)e^{\frac{2t\sqrt{m_2 B_{\text{orb}}(1-b)}}{\sqrt{A}}} + \left(e^{\frac{4t\sqrt{m_2 B_{\text{orb}}(1-b)}}{\sqrt{A}}} + 1\right)(b+1)}. \tag{4.39}$$

So, now we have the final analytical solution (4.39) for $\cos\theta$ and for the canonical momentum p_θ (4.34). The numerical confirmation of the analytical solutions and the phase portrait $\{\theta, p_\theta\}$ are presented in Figs. 16, 17, where the axis for momentum p_θ is scaled for the maximum value $p_\theta = 30\ \left[\text{kg}\cdot\text{m}^2/\text{s}\right]$.

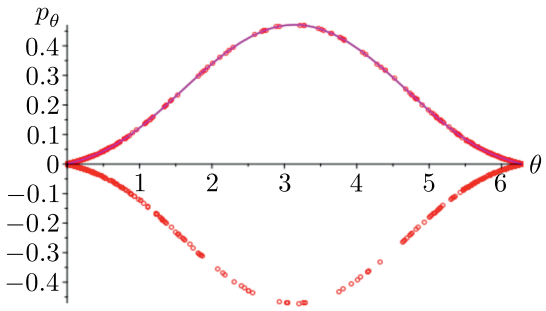

Fig. 16. The homoclinic trajectory of case 3: the magenta line is the analytical solution, and the red dots indicate numerical calculations

4.4. Small time-perturbations and chaotization of motion

The analytical solutions obtained above for the homo- and heteroclinic trajectories (cases 1–3) allow analyzing the possible chaotization of the magnetic Lagrange gyrostat dynamics.

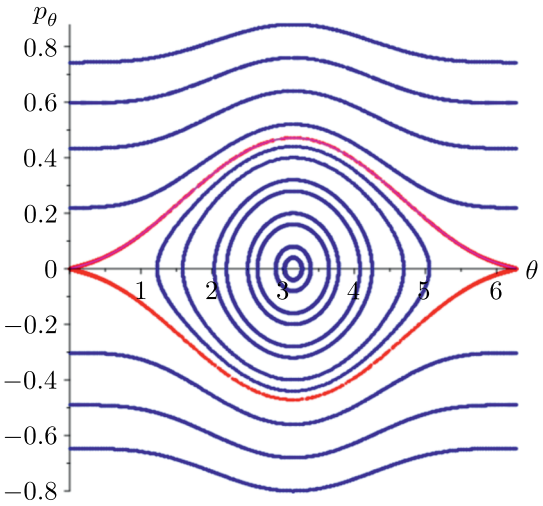

Fig. 17. The phase portrait of case 3: the upper heteroclinic trajectory (the magenta line) is analytical, and the lower trajectory (the red line) is numerical

As a short example, we can consider the homoclinic (heteroclinic) chaos arising under the action of small harmonic perturbations changing the value of the magnet dipole moment terms:

$$m_1 = \overline{m}_1(1 + \varepsilon \sin(\omega_m t)); \quad m_2 = \overline{m}_2(1 + \varepsilon \sin(\omega_m t)), \tag{4.40}$$

where ε is the small dimensionless parameter, and ω_m is the frequency of perturbing oscillations. The perturbation (4.40) can model parasitic oscillations in electrical circuits in magnetic coils of the satellite control system.

The presence of the perturbations (4.40) changes the equation for the canonical momentum p_θ, where the small addition proportional to ε appears on the right-hand side:

$$g(\theta,\, t) = 2\varepsilon \left(\overline{m}_2 B_{\text{orb}} \cos\theta + \frac{\overline{m}_1 B_{\text{orb}}}{2} \right) \sin\theta \sin(\omega_m t). \tag{4.41}$$

The equation for the angle θ has not any additions, the equation retains its unperturbed form:

$$\dot{\theta} = f(p_\theta) = \frac{p_\theta}{A}. \tag{4.42}$$

In the type of perturbed system considered above, the following Melnikov function can be written (where $\overline{\theta}(t)$ and $\overline{p}_\theta(t)$ are the homoclinic (heteroclinic) solutions obtained in the previous subsections):

$$M(\tau) = \int\limits_{-\infty}^{+\infty} g(\overline{\theta}(t),\, t + \tau) f(\overline{p}_\theta(t))\, dt. \tag{4.43}$$

On the basis of the concrete form of functions f and g we take:

$$M(\tau) = \frac{2\varepsilon}{A} \int\limits_{-\infty}^{+\infty} \left(\overline{m}_2 B_{\text{orb}} \cos\overline{\theta}(t) + \frac{\overline{m}_1 B_{\text{orb}}}{2} \right) \sin\overline{\theta}(t) \sin(\omega_m(t + \tau))\overline{p}_\theta(t)\, dt. \tag{4.44}$$

After trigonometric transformations, up to a multiplier we obtain:

$$M(\tau) = M_c(\tau) + M_s(\tau), \tag{4.45}$$

where

$$\begin{cases} M_s(\tau) = \cos(\omega_m \tau) \displaystyle\int_{-\infty}^{+\infty} \left(\overline{m}_2 B_{\text{orb}} \cos\overline{\theta}(t) + \frac{\overline{m}_1 B_{\text{orb}}}{2} \right) \sin\overline{\theta}(t) \overline{p}_\theta(t) \sin(\omega_m t)\, dt; \\ M_c(\tau) = \sin(\omega_m \tau) \displaystyle\int_{-\infty}^{+\infty} \left(\overline{m}_2 B_{\text{orb}} \cos\overline{\theta}(t) + \frac{\overline{m}_1 B_{\text{orb}}}{2} \right) \sin\overline{\theta}(t) \overline{p}_\theta(t) \cos(\omega_m t)\, dt. \end{cases} \tag{4.46}$$

If we plot the integrands of (4.46) on the basis of the analytical solutions of case 1, then we obtain the graphs shown in Fig. 18.

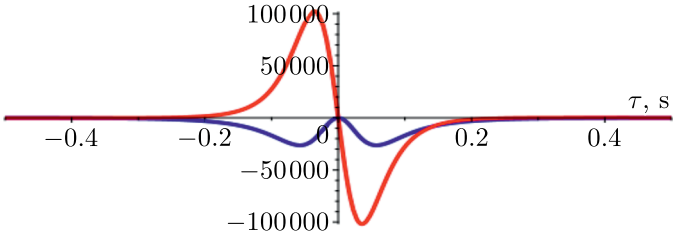

Fig. 18. Graphs of the integrands of M_s (blue) and M_c (red) in case 1

The form of the integrand M_s (Fig. 18) corresponds to an even function, therefore, the improper integral M_s will have nonzero value $\overline{M}_s$. The integrand M_c corresponds to an odd function, therefore, integral M_c gives zero value. Then the Melnikov function takes the harmonic form:

$$M(\tau) = \overline{M}_s \cos(\omega_m \tau). \tag{4.47}$$

The harmonic form (4.47) has an infinite number of simple zeros, therefore, homoclinic chaos will arise in the system.

Also, in cases 2 and 3 dynamical chaos will be initiated by perturbations (4.40), which can be shown by analogy. In addition, it is quite illustrative to show the Poincaré sections $\{\theta, p_\theta\}$ for all three cases of phase portraits under the action of the perturbation (4.40) (Figs. 19–21).

So, for all three cases we see chaotic dynamics under the action of small perturbations, which was illustrated by the Melnikov function and Poincaré sections.

4.5. New possibilities in remote sensing

New dynamical possibilities for the magnetic Lagrange gyrostat under changes in the own magnetic dipole moment **m** allow one to synthesize nutational-precessional motions that can be applied to a more accurate scanning in the remote sensing tasks (Fig. 4). Varying the control of the dipole moment can change the parameters of nutational and precessional oscillations, and the internal torque of the rotor spin-up can control the intrinsic rotation angle. In our modeling, the simplest variant of this method was considered when we added only one additional second harmonic to the potential (4.3) and generated a simple form of the internal torque (3.11). However, even this simplest generalizing case allows finding appropriate motion regimes (Fig. 22)

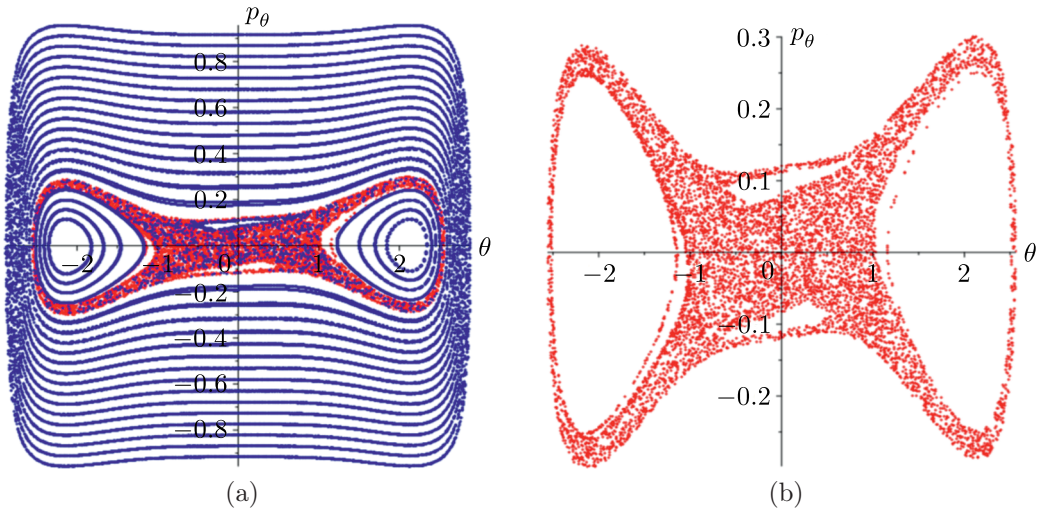

Fig. 19. The Poincaré section and the heteroclinic area in case 1 at $\varepsilon = 0.1$ and $\omega_m = 5.5$ [1/s]

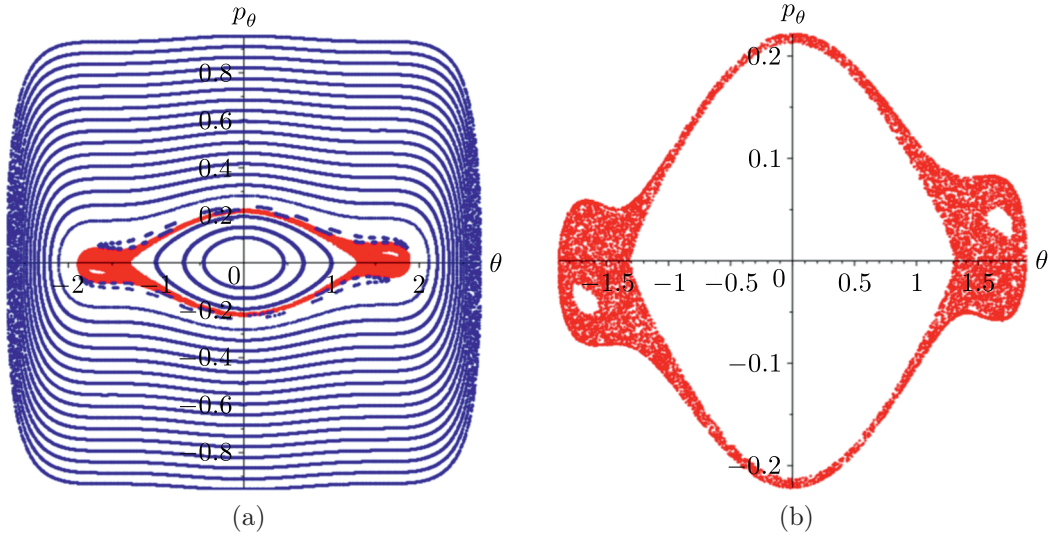

Fig. 20. The Poincaré section and the heteroclinic area in case 2 at $\varepsilon = 0.1$ and $\omega_m = 5.5$ [1/s]

and parameters (Table 5). These regimes are characterized by small values of precession and intrinsic rotation oscillations, which can form a concentrated scanning strip.

As we can see from Fig. 23, we have a quite concentrated scanning strip as compared to the wide view variant (Fig. 6). So, the development of this approach can be quite useful in space missions with remote sensing satellites, especially in cases of nanosatellites with simple sets of control actuators. Certainly, such a development is a research problem in its own right.

Table 5. Parameters for calculation (Figs. 22, 23)

A $[\mathrm{kg}\cdot\mathrm{m}^2]$	C_n $[\mathrm{kg}\cdot\mathrm{m}^2]$	C_r $[\mathrm{kg}\cdot\mathrm{m}^2]$	$m_1 B_{\mathrm{orb}}$ $[\mathrm{N}\cdot\mathrm{m}]$	$m_1 B_{\mathrm{orb}}$ $[\mathrm{N}\cdot\mathrm{m}]$	p_ψ $[\mathrm{kg}\cdot\mathrm{m}^2/\mathrm{s}]$	p_φ $[\mathrm{kg}\cdot\mathrm{m}^2/\mathrm{s}]$	p_δ $[\mathrm{kg}\cdot\mathrm{m}^2/\mathrm{s}]$	Ω [1/s]	ω_δ [1/s]	G $[\mathrm{kg}\cdot\mathrm{m}^2/\mathrm{s}]$	$M_{\mathrm{spin}}T_{\mathrm{spin}}$ $[\mathrm{kg}\cdot\mathrm{m}^2/\mathrm{s}]$
0.5	0.6	0.2	1	−45.85	0.001	0.001	1.48	0.001	10	0.005	−1.48

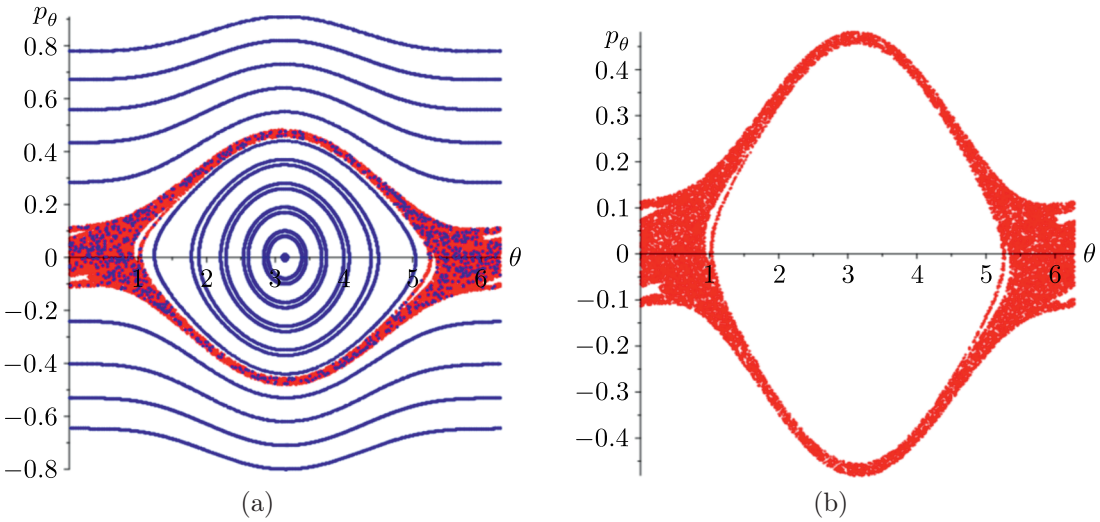

Fig. 21. The Poincaré section and the heteroclinic area in case 3 at $\varepsilon = 0.1$ and $\omega_m = 5.5$ [1/s]

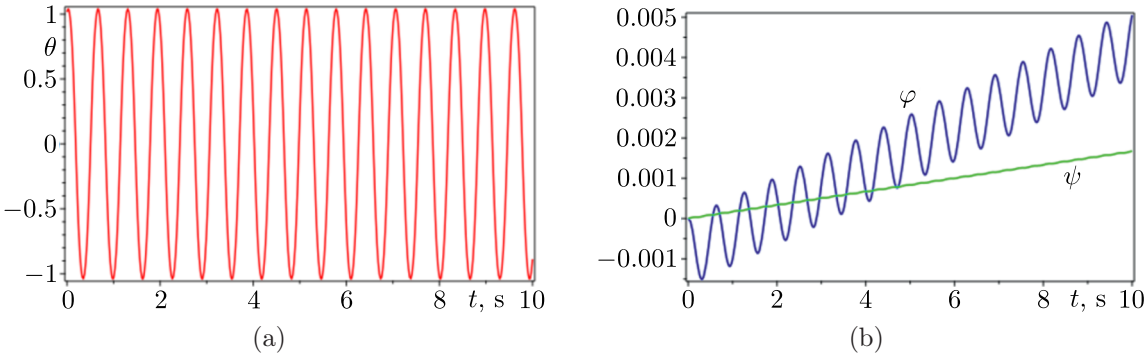

Fig. 22. Time dependencies for the nutation θ (red), the intrinsic rotation φ (blue), the precession ψ (green) angles during hypothetical remote sensing process with the torque (3.11)

5. Conclusion

In this paper, the attitude dynamics of the Lagrange gyrostat was considered. A dynamical analogy of the heavy Lagrange gyrostat and the magnetic Lagrange gyrostat on the circular equatorial orbit in the geomagnetic field was shown. Analytical solutions for a homoclinic and heteroclinic phase trajectory were obtained. These analytical solutions correspond to three cases of separatrices in different forms of phase portraits. Using the solutions obtained, dynamical chaos was analyzed with the help of the Melnikov function and Poincaré sections of the phase space of the perturbed system. A practical application of the Lagrange gyrostat was proposed within the framework of space flight mechanics. The results obtained can be especially applicable for small spacecraft and nanosatellites of space remote sensing constellations.

Conflict of interest

The authors declare that they have no conflicts of interest.

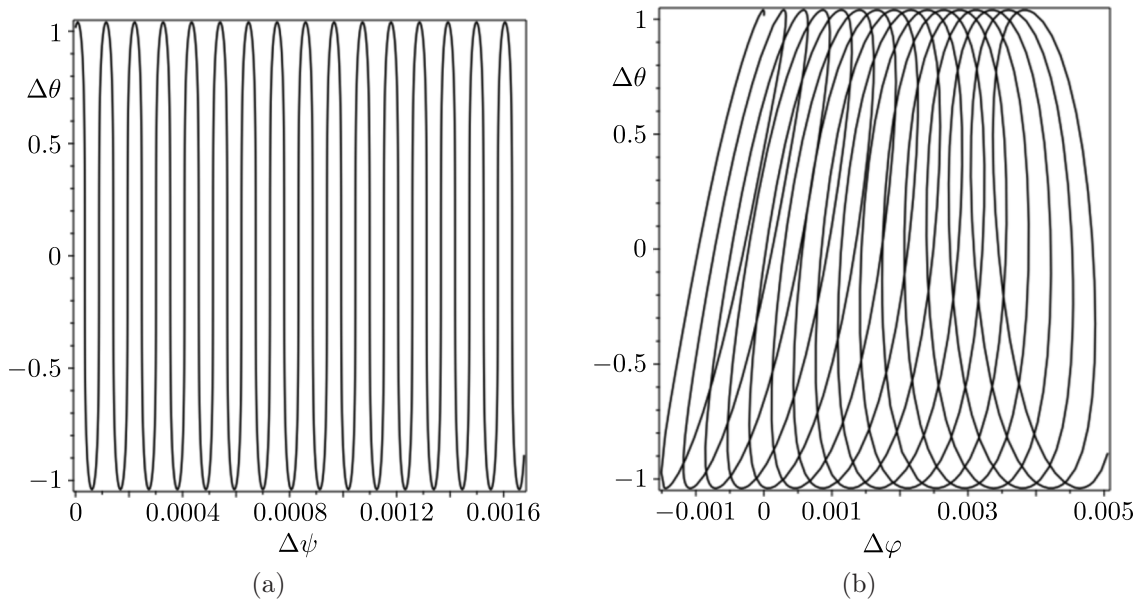

Fig. 23. The coverage of the scanning strip during the angular motion: (a) the strip $\{\Delta\psi, \Delta\theta\}$ and (b) the intrinsic rotation hodograph $\{\Delta\varphi, \Delta\theta\}$

References

[1] Borisov, A. V. and Mamaev, I. S., *Rigid Body Dynamics,* De Gruyter Stud. Math. Phys., vol. 52, Berlin: De Gruyter, 2018.

[2] Borisov, A. V. and Mamaev, I. S., Euler – Poisson Equations and Integrable Cases, *Regul. Chaotic Dyn.,* 2001, vol. 6, no. 3, pp. 253–276.

[3] Borisov, A. V. and Mamaev, I. S., Generalization of the Goryachev – Chaplygin Case, *Regul. Chaotic Dyn.,* 2002, vol. 7, no. 1, pp. 21–30.

[4] Borisov, A. V., Kilin, A. A., and Mamaev, I. S., Chaos in a Restricted Problem of Rotation of a Rigid Body with a Fixed Point, *Regul. Chaotic Dyn.,* 2008, vol. 13, no. 3, pp. 221–233.

[5] Bizyaev, I. A., Borisov, A. V., and Mamaev, I. S., Generalizations of the Kovalevskaya Case and Quaternions, *Proc. Steklov Inst. Math.,* 2016, vol. 295, no. 1, pp. 33–44; see also: *Tr. Mat. Inst. Steklova,* 2016, vol. 295, pp. 41–52.

[6] Borisov, A. V., Ryabov, P. E., and Sokolov, S. V., On the Existence of Focus Singularities in One Model of a Lagrange Top with a Vibrating Suspension Point, *Dokl. Math.,* 2020, vol. 102, no. 3, pp. 468–471; see also: *Dokl. Akad. Nauk,* 2020, vol. 495, no. 1, pp. 26–30.

[7] Ratiu, T. and van Moerbeke, P., The Lagrange Rigid Body Motion, *Ann. Inst. Fourier (Grenoble),* 1982, vol. 32, no. 1, pp. 211–234.

[8] Zhuravlev, V. F. and Petrov, A. G., The Lagrange Top and the Foucault Pendulum in Observed Variables, *Dokl. Phys.,* 2014, vol. 59, no. 1, pp. 35–39; see also: *Dokl. Akad. Nauk,* 2014, vol. 454, no. 2, pp. 168–172.

[9] Petrov, A. G. and Sanduleanu, S. V., The Lagrange Top in Terms of Observable Variables, *Dokl. Phys.,* 2016, vol. 61, no. 10, pp. 517–520; see also: *Dokl. Akad. Nauk,* 2016, vol. 470, no. 6, pp. 658–661.

[10] Ishikawa, G., An Elliptic Fibration Arising from the Lagrange Top and Its Monodromy, *J. Geom. Phys.,* 2025, vol. 216, Paper No. 105595, 22 pp.

[11] Gutnik, S. A. and Sarychev, V. A., Application of Symbolic Computation Methods for Investigation of Stationary Motions of an Axisymmetric Satellite, *Program. Comput. Softw.,* 2018, vol. 44, no. 2, pp. 94–99; see also: *Programmirovanie,* 2018, no. 2, pp. 96–101.

[12] Akulenko, L. D., Zinkevich, Ya. S., Kozachenko, T. A., and Leshchenko, D. D., The Evolution of the Motions of a Rigid Body Close to the Lagrange Case under the Action of an Unsteady Torque, *J. Appl. Math. Mech.,* 2017, vol. 81, no. 2, pp. 79–84; see also: *Prikl. Mat. Mekh.,* 2017, vol. 81, no. 2, pp. 115–122.

[13] Leshchenko, D., Ershkov, S., and Kozachenko, T., Rotations of a Rigid Body Close to the Lagrange Case under the Action of Nonstationary Perturbation Torque, *J. Appl. Comput. Mech.,* 2022, vol. 8, no. 3, pp. 1023–1031.

[14] Krasilnikov, P. S. and Amelin, R. N., On Saturn's Rotation Relative to a Center of Mass under the Action of the Gravitational Moments of the Sun and Jupiter, *Cosmic Research,* 2016, vol. 54, no. 2, pp. 127–133; see also: *Kosmicheskie Issledovaniya,* 2016, vol. 54, no. 2, pp. 135–142.

[15] Zabolotnov, Yu. M., The Resonance Motions of a Statically Stable Lagrange Top at Small Nutation Angles, *J. Appl. Math. Mech.,* 2016, vol. 80, no. 4, pp. 302–310; see also: *Prikl. Mat. Mekh.,* 2016, vol. 80, no. 4, pp. 432–443.

[16] Chernousko, F. L., Akulenko, L. D., and Leshchenko, D. D., *Evolution of Motions of a Rigid Body about Its Center of Mass,* Cham: Springer, 2017.

[17] Dawson, S. R., Dullin, H. R., and Nguyen, D. M. H., The Harmonic Lagrange Top and the Confluent Heun Equation, *Regul. Chaotic Dyn.,* 2022, vol. 27, no. 4, pp. 443–459.

[18] Aslanov, V. S. and Timbay, I. A., Action-Angle Canonical Variables for the Motion of a Rigid Body under the Action of a Biharmonic Torque, *Mech. Solids,* 2003, vol. 38, no. 1, pp. 13–23; see also: *Izv. Akad. Nauk SSSR. Mekh. Tverd. Tela,* 2003, no. 1, pp. 17–30.

[19] Ryabov, P. E. and Sokolov, S. V., Bifurcation Diagram of the Model of a Lagrange Top with a Vibrating Suspension Point, *Mathematics,* 2023, vol. 11, no. 3, Art. 533, 8 pp.

[20] Belichenko, M. V., On the Stability of Pendulum-Type Motions in the Approximate Problem of Dynamics of a Lagrange Top with a Vibrating Suspension Point, *Russian J. Nonlinear Dyn.,* 2018, vol. 14, no. 2, pp. 243–263.

[21] Markeev, A. P., On the Motion of a Heavy Dynamically Symmetric Rigid Body with Vibrating Suspension Point, *Mech. Solids,* 2012, vol. 47, no. 4, pp. 373–379; see also: *Izv. Akad. Nauk. Mekh. Tverd. Tela,* 2012, no. 4, pp. 3–10.

[22] Krasilnikov, P., Gurina, T., and Svetlova, V., Bifurcation Study of a Chaotic Model Variable-Length Pendulum on a Vibrating Base, *Int. J. Non-Linear Mech.,* 2018, vol. 105, pp. 88–98.

[23] Kholostova, O. V., On the Stability of the Specific Motions of a Heavy Rigid Body due to Fast Vertical Vibrations of one of Its Points, *Nelin. Dinam.,* 2015, vol. 11, no. 1, pp. 99–116 (Russian).

[24] Kozlov, V. V. and Treshchev, D. V., Nonintegrability of the General Problem of Rotation of a Dynamically Symmetric Heavy Rigid Body with a Fixed Point: 1, *Vestn. Mosk. Univ. Ser. 1. Mat. Mekh.,* 1985, no. 6, pp. 73–81 (Russian).

[25] Kozlov, V. V. and Treshchev, D. V., Nonintegrability of the General Problem of Rotation of a Dynamically Symmetric Heavy Rigid Body with a Fixed Point: 2, *Mosc. Univ. Mech. Bull.,* 1986, vol. 41, no. 1, pp. 11–16; see also: *Vestn. Mosk. Univ. Ser. 1. Mat. Mekh.,* 1986, no. 1, pp. 39–44.

[26] Holmes, Ph. J. and Marsden, J. E., Horseshoes and Arnol'd Diffusion for Hamiltonian Systems on Lie Groups, *Indiana Univ. Math. J.,* 1983, vol. 32, no. 2, pp. 273–309.

[27] Aslanov, V. S. and Doroshin, A. V., Two Cases of Motion of an Unbalanced Gyrostat, *Mech. Solids,* 2006, vol. 41, no. 4, pp. 29–39; see also: *Izv. Akad. Nauk. Mekh. Tverd. Tela,* 2006, no. 4, pp. 42–55.

[28] Tikhonov, A. A., The Integrable Case in the Gyrostat Attitude Motion in the Gravitational and Magnetic Earth's Fields, *Vestn. Udmurtsk. Univ. Mat. Mekh. Komp. Nauki,* 2009, no. 2, pp. 89–96 (Russian).

[29] Chebanov, D. and Salas, J. A., On the Stability of Permanent Rotations of a Chain of Two Lagrange Gyrostats in a Central Gravitational Field, in *Proc. of the 2016 ASME International De-*

sign Engineering Technical Conferences and Computers and Information in Engineering Conference (Charlotte, N.C., USA, Aug 2016): Vol. 6, UNSP V006T09A001.

[30] Bogoyavlenskii, O. I., Integrable Euler Equations on Lie Algebras Arising in Problems of Mathematical Physics, *Math. USSR-Izv.,* 1985, vol. 25, no. 2, pp. 207–257; see also: *Izv. Akad. Nauk SSSR Ser. Mat.,* 1984, vol. 48, no. 5, pp. 883–938.

[31] Makeyev, N. N., Stability of Regular Precession a Gyrostat-Magnetic in a Magnetic Field, *Vestn. Permsk. Univ. Mat. Mekh. Informatika,* 2014, no. 4 (27), pp. 35–42 (Russian).

[32] Gutnik, S. A. and Sarychev, V. A., Application of Computer Algebra Methods for Investigation of Stationary Motions of a Gyrostat Satellite, *Program. Comput. Softw.,* 2017, vol. 43, no. 2, pp. 90–97; see also: *Programmirovanie,* 2017, no. 2, pp. 35–44.

[33] Doroshin, A. V., Attitude Dynamics of Gyrostat-Satellites under Control by Magnetic Actuators at Small Perturbations, *Commun. Nonlinear Sci. Numer. Simul.,* 2017, vol. 49, pp. 159–175.

[34] Doroshin, A. V., Analytical Solutions for Dynamics of Dual-Spin Spacecraft and Gyrostat-Satellites under Magnetic Attitude Control in Omega-Regimes, *Internat. J. Non-Linear Mech.,* 2017, vol. 96, pp. 64–74.

[35] Ovchinnikov, M. Yu. and Roldugin, D. S., A Survey on Active Magnetic Attitude Control Algorithms for Small Satellites, *Prog. Aerosp. Sci.,* 2019, vol. 109, Art. 100546.

[36] Ovchinnikov, M. Yu. and Roldugin, D. S., Magnetic Attitude Control and Periodic Motion for the In-Orbit Rotation of a Dual-Spin Satellite, *Acta Astronaut.,* 2021, vol. 186, pp. 203–210.